Arch. Metall. Mater. **69** (2024), 2, 563-570

DOI: https://doi.org/10.24425/amm.2024.149784

M.F. KALKAN[1*], M. ALADAG[2], K.J. KURZYDLOWSKI[2], N.F. YILMAZ[1,4], A. YAVUZ[3]

COMPARATIVE STUDY ON DIFFERENT CNN ARCHITECTURES DEVELOPED ON MICROSTRUCTURAL CLASSIFICATION IN Al-Si ALLOYS

Recent advances in artificial intelligence have opened up new avenues for microstructure characterization, notably in metallic materials. Physical and mechanical properties generally depend on the microstructure of the metallic material. On the other hand, microstructural characterization takes time and calls for specific techniques that don't always lead to conclusive results quickly. To address this issue, this research focuses on the application of artificial intelligence approaches to microstructural categorization. We demonstrate the advantages of the AI approach using an example of Al-Si alloy, a material that is widely employed in a variety of industries. To specify a suitable convolutional neural network (CNN) approach for the microstructural classification of the Al-Si alloy, CNN models were trained and compared using DenseNet201, Inception v3, InceptionResNetV2, ResNet152V2, VGG16, and Xception architectures. Resulting from the comparison, it was determined that the developed supervised transfer learning model can execute the microstructural classification of Al-Si alloy microstructural images. This paper is an attempt to advance methods of microstructure recognition/classification/characterization by using Deep Learning approaches. The significance of the established model is demonstrated and its accordance with the literature data. Also, necessity is shown of developing material models and optimization through systematic microstructural investigation, production conditions, and material attributes.

Keywords: Artificial intelligence; Microstructural characterization; Al-Si alloy; Convolutional neural network (CNN); Material classification

1. Introduction

Microscopic studies play a significant role in material quality control. The most complicated mechanism is microstructural characterization and classification. Both qualitative and quantitative microstructural characteristics are needed. Out of these two characteristics, the qualitative one is fundamental, as for qualitative one needs to know the type of microstructure to select proper quantitative characteristics [1]. For example, a number of phases can be determined in qualitative analysis, and subsequently, volume fractions of these phases can be determined. The person who interprets microstructural studies has to have the necessary training and expertise [2]. It should be noted that qualitative analysis of images of microstructure is generally very challenging. This is so for several reasons. First, there are large numbers of engineering metals, polymers, ceramics, and their compositions. Second, there is a considerable degree of variation in the size/shape of the feature, the typical type of a given type of microstructure. Thirdly, 3-D structures are typically transformed into 2-D images through projection. In this situation, qualitative analysis is very much subjective and a correct description of the type of microstructural features can be performed effectively by a well-trained specialist. Each type of material has distinct microstructural features, like crystallites, grains, phases, and reinforcements. Image-based artificial intelligence research has long been a popular issue in the medical business. Yet, this area is only beginning to acquire traction in the realm of engineered materials research. Artificial intelligence and image processing studies of microstructure characterization and classification in the field of materials have gained attention in the literature as a result of data science and information technology advancements, as well as the significance of the topic [3]. The integration of computer vision and machine learning techniques has led to remarkable outcomes in the automatic recognition of dendritic microstructures within micrographs. This achievement has been marked by its impressive accuracy and holds promise

[1] GAZIANTEP UNIVERSITY, FACULTY OF ENGINEERING, DEPARTMENT OF MECHANICAL ENGINEERING, 27310, SEHITKAMIL, GAZIANTEP, TURKIYE
[2] BIALYSTOK UNIVERSITY OF TECHNOLOGY, FACULTY OF MECHANICAL ENGINEERING, WIEJSKA 45C, 15-351 BIALYSTOK, POLAND
[3] GAZIANTEP UNIVERSITY, FACULTY OF ENGINEERING, DEPARTMENT OF METALLURGICAL AND MATERIALS ENGINEERING, 27310, SEHITKAMIL, GAZIANTEP, TURKIYE
[4] HASAN KALYONCU UNIVERSITY, BOARD OF TRUSTEES, 27410 GAZIANTEP, TURKEY

* Corresponding author: nfyilmaz@gantep.edu.tr

for diverse applications in material characterization [4]. These advancements involve the encoding of microstructural image data through the utilization of features or convolutional neural networks (CNNs). As a result, machine learning algorithms leverage this densely encoded data, revealing complex material correlations in the process [5].

The popularity of artificial intelligence techniques and tools in academia and industry has just begun at the beginning of the 21st century. The starting point of this popularity is based on people fully discovering the benefits of machine learning to solve problems. This popularity has continued to accelerate with the development of deep learning in the last decade. With the use of deep learning and image processing methods together, the use of images as datasets in artificial intelligence applications has become widespread. Many studies are conducted in academia on the creation of diagnosis and treatment approaches, particularly in the medical context. Research on this topic in the realm of material engineering is gaining traction. Material informatics necessitates the utilization of data-driven methods for microstructure identification [6]. Researchers proved the use of computer vision in materials science, including machine learning for microstructure recognition [7,8]. For example, Chowdhury et al. [9] used computer vision and algorithms such as support vector machine (SVM), random forest, and deep neural network to classify dendritic microstructures. Most studies in the literature have utilized statistics-based machine learning models. While these models have demonstrated success, they might not be suitable for multi-class classification in big data collection. In such cases, convolutional neural network (CNN) models have promised relatively outstanding accuracy from a perspective [10,11].

From this end, solid evidence in recent literature suggests the capability to reconstruct microstructures using data-driven approaches. For example, [12,13] used image processing techniques and deep learning to classify with reasonable accuracy, while Shen et al. [14] used deep learning to classify martensite/ferrite phases and their fraction. Additionally, Feng et al. [15] proposed a deep learning framework to characterize the microstructure of metals by supporting the periodic data table knowledge and, therefore, enabled to obtaining of more characteristic information from microstructure images.

Architectures such as, VGG16 [16], Xception [17], Resnet152 and InceptionResNetV2 [18], InceptionV3 [19], and DenseNet201 [20] are used in computer vision applications. In the present study, microstructural phase structures of Al-Si alloy datasets with various architectures were generated using a pre-trained CNN model. This was accomplished by analyzing the literature and subsequently classifying the microstructural phase structures of Al-Si alloys. The best model by comparing different architectures and using data preparation, training, categorization, and assessment. The models were trained over the dataset using image augmentation techniques and were assessed by using an independent test set. The results were analyzed using a heatmap of the confusion matrix.

2. Materials and methods

The specifics of Keras-based CNN pre-trained architectures used for the categorization of general phase structures of Al-Si alloys obtained as part of the study are discussed in this section. The entire operation is broken down into four fundamental parts. Data preparation, data training, data categorization, and data assessment are the phases involved.

2.1. Dataset preparation

In the scope of the investigation, a dataset with equal amounts for three classes was created. The dataset for the hypoeutectic Al-Si alloy mostly consisted of microstructure pictures collected from laboratory tests done as part of our research and microscopic photos taken from the literature [21-24].

Microstructure pictures for the hypereutectic Al-Si alloy were created using references from the literature [23,25-31], whereas microstructure photos for the eutectic Al-Si alloy were created using references from the literature [21,28,32-35]. Images were collected and resized as 180×180 pixels. Images were taken regardless of magnification in order for the model to be applicable to all microscope objectives. Three different datasets were prepared for this study as learning, validation, and test. The number of 380 resized images of the learning dataset, 79 resized images of the validation dataset, and 300 resized images of the test dataset were used in this current study. It is important to note that the selected images were entirely utilized to identify the type of microstructure. Consequently, the provided dataset does not encompass the entire range of microstructure properties at an identical scale.

2.2. Model architecture

The comparison of VGG16, Xception, Resnet152, InceptionV3, InceptionResNetV2, and DenseNet201 CNN architectures for the classification of general microstructural phases of Al-Si alloys is a focal point in this study. These selected models were built on the Keras library with a TensorFlow backend. These architectures were used as pre-trained models. Models were initialized with the pre-trained weights, and we built a custom classification head on top of the standard model to fine-tune the network for unique goal of this study. The classification head was made up of a single fully connected layer with 64 neurons, activated using Rectified Linear Unit (ReLU) activation, followed by a dropout layer with a rate of 0.5. The final output layer is composed of three neurons representing our three classes, and softmax activation is utilized to distribute probability between them.

2.3. Data training

The construction of CNNs was carried out over the dataset. The models in the current study were compiled with a categorical cross-entropy loss function and Adam optimizer. The models were trained using the *"fit_generator"* function for 50 epochs, with a batch size of 16. Early stopping were applied with a patience of 5 epochs to prevent overfitting. Also image augmentation method was used to supply more amount of data for the CNN architectures to create the more productive deep neural network models [36]. In the image augmentation approach, two non-random procedures were used: rescaling, which included dividing the pixel values by 255 to scale them in the range from 0 and 1, and fill mode, which involved filling the pixels in the newly produced regions after the picture was altered. Shear, zoom, horizontal and vertical flip, width and height shift, and brightness were also employed at random. Selection of the CNN architectures was carried out depend on the image size used in this study. CNNs models requires a large number of data to train the tasks successively. Because of that reason ImageNet was used to train a pre-trained models. ImageNet, with over 20.000 categories, was leveraged as a source of pre-trained models to increase model performance and training time. The general training structure scheme of the prepared models is given in Fig. 1.

2.4 Model evaluation

To assess the trained model's performance, an independent test set of 300 images that were not utilized for training or validation was employed. The test set was likewise supplemented

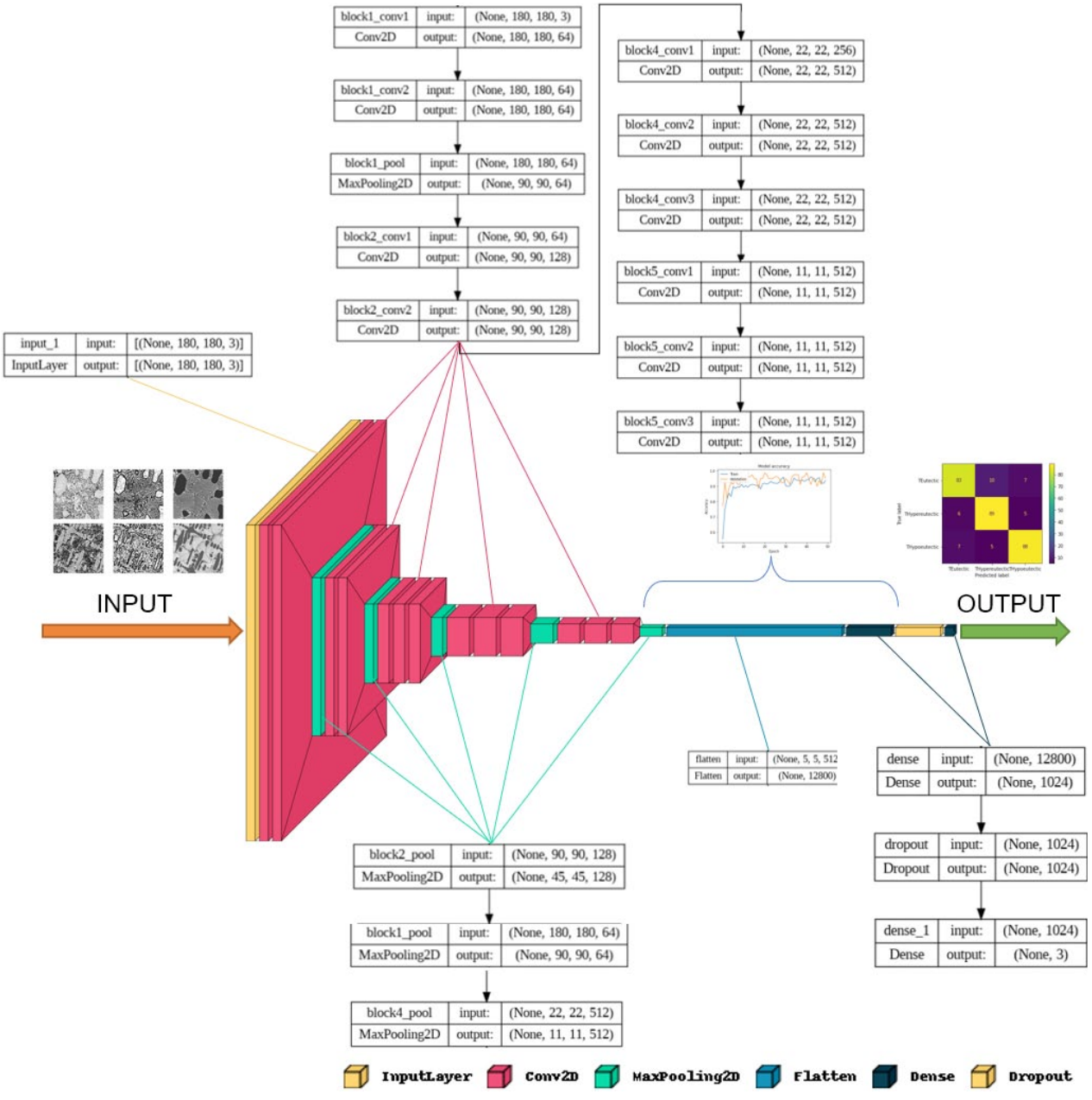

Fig. 1. Training Structure Scheme

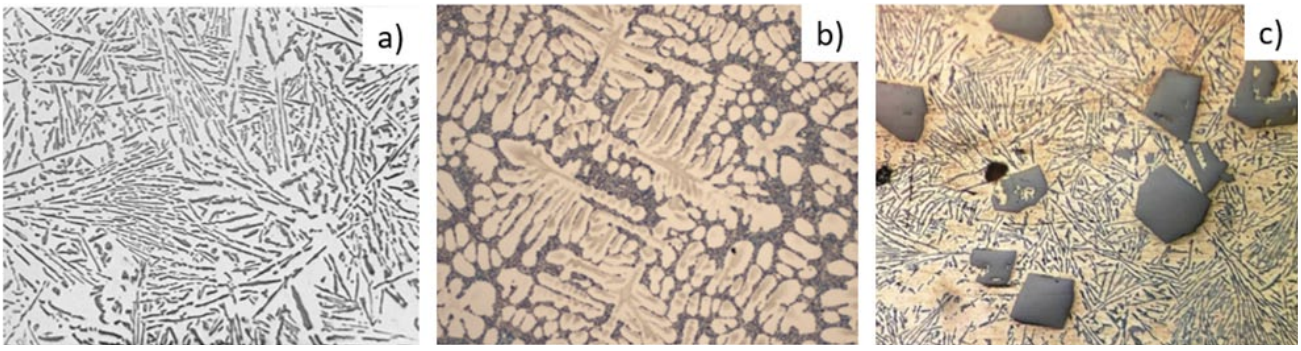

Fig. 2. General microstructural views of a) Eutectic Al-Si alloy [35]; b) Hypoeutectic Al-Si alloy [24]; and c) Hypereutectic Al-Si alloy [31]

using the same data augmentation techniques as the training set. The trained model was used to predict the test set and compute evaluation measures such as accuracy, precision, recall, F1-score, AUC (area under curve) and confusion matrix. Precision, recall and F1-score values were calculated from confusion matrices. AUC was determined by using Scikit-Learn library. To visualize the model's classification performance, the confusion matrix was presented as a heatmap.

3. Result and discussion

Al-Si microstructures fluctuate in the Al-Si alloy phase diagram depending on the quantity of silicon and the cooling rate. Al-Si microstructures are classified into three types based on this microstructural change: eutectic, hypoeutectic, and hypereutectic. Fig. 2a shows the eutectic Al-Si microstructure.

Approximately 12% in the eutectic Al-Si microstructure. It is the structure that comprises 7 silicon, and in general, acicular silicon is disseminated into the Al matrix. The silicon phase might appear more regular or irregular depending on the cooling rate of this structure. The silicon content of the hypo-eutectic Al-Si microstructure (shown in Fig. 2b) is smaller than that of the eutectic Al-Si microstructure. The Si phase is distributed in the Al matrix and has a primarily round structure in this kind of Al-Si alloy. Hypereutectic

Al-Si alloys are those that contain more water than eutectic Al-Si alloys. The Si phase is insoluble in such alloys and accumulates in the Al matrix. Because the Si content in the alloy is high, the phase structure is commonly plate or acicular. Fig. 3b

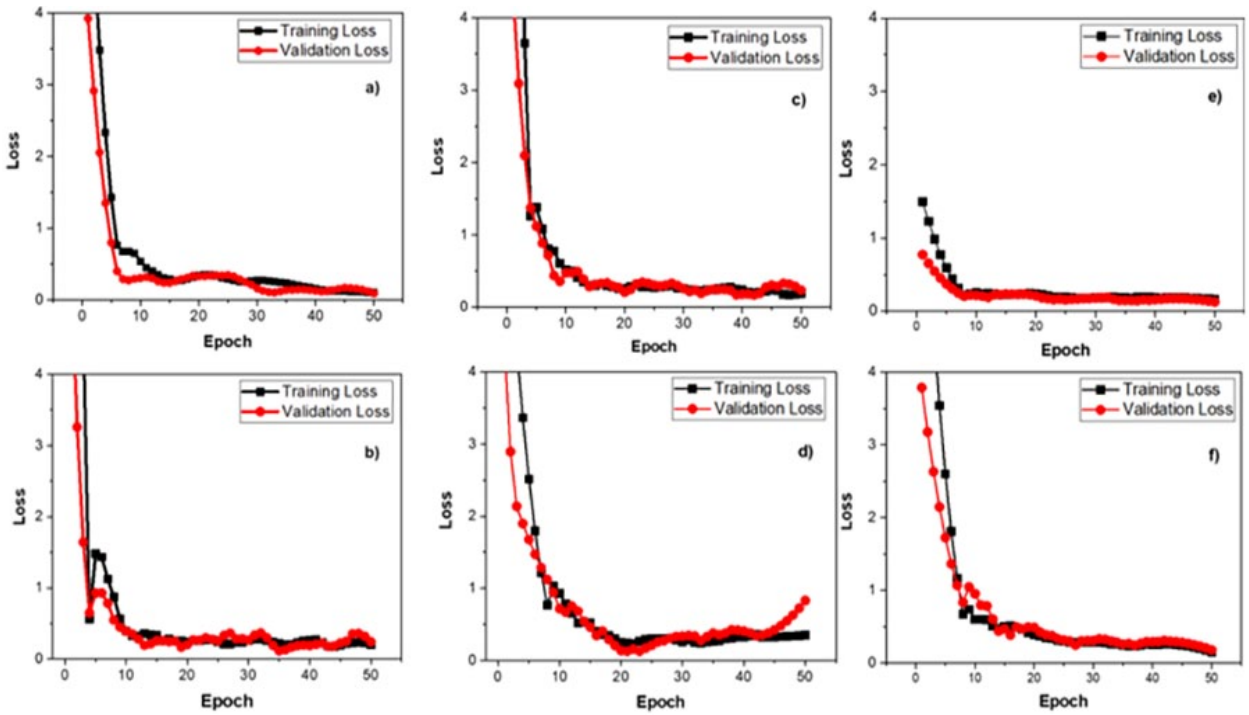

	Xception	VGG16	InceptionV3	ResNet152V2	InceptionResNetV2	DenseNet201
Final Training Loss %	16.92	15.92	24.15	54.52	21.78	09.06
Final Validation Loss %	22.98	13.39	18.68	70.40	16.95	12.78

Fig. 3. Training and validation loss graphs for using a) Xception, b) VGG16, c) Resnet152V2, d) Resnet152V2, e) InceptionResNetV2, f) DenseNet201 architectures

depicts the common microstructure of the hypereutectic Al-Si morphology. The changes that may occur in the three different morphologies mentioned are due to the additive elements that can be added and the cooling rate. However, it is difficult to compare these structures in different magnifications taken under the microscope.

By providing those above-mentioned images, the training validation and lost histories were plotted for each training models. In Figs. 3a, 3b, 3c and 3e, that is, the models DenseNet201, Inception_v3; InceptionResNetV2, VGG16, the training curves came up the maximum point of training and validation loss. Figs. 3b and 3c, Inception_v3 and InceptionResNetV2, are more identical. In Fig. 3f the Xception model, the losses are in the decreasing tendency. However, in Fig. 3d that is in ResNet152V2, overfitting occurred in the given epoch. It was observed that ResNet152V2 was the model with the highest loss in both training and validation stages. However, it was seen that DenseNet201 presented the lowest loss in the training and validation stages. Even so, during training and validation, the Xception and DenseNet201 designs were shown to be somewhat overfitting.

The final training, validation and test accuracy values of the models were plotted in Fig. 4. An accuracy score of 100% means that the model correctly classified all items in the dataset. In three steps, the DenseNet201 model with the lowest training and validation loss after 50 epochs was shown to have the maximum efficiency outcomes. However, when the accuracy values were considered, it was discovered that the validation loss being greater than the training loss in the DenseNet201 model had no detrimental effect. This suggests that this model may be the best performing model overall. Depending on the test performance, the models with the best performance were InceptionResNetV2 with 93.33% efficiency, ResNet152V2 with 93.33% efficiency, Xception with 89.33% efficiency, VGG16 with 88.33% efficiency and InceptionV3 with 87% efficiency.

It is well recognized in the literature that as the depth of the model connected to this circumstance develops, so does the complexity, learning of small details, and performance [37].

TABLE 1

The parameter number of prepared models

Model Name	Total Parameters
Xception	96.363.051
VGG16	27.825.98
ResNet152V2	133.833.219
InceptionV3	55.361.315
InceptionResNetV2	79.506.659
DenseNet201	67.478.083

However, this is just one of several elements that influence model performance, including hardware, data set, method, and hyperparameters [38]. The model requires more data as the number of parameters rises. In this situation, a decline in model performance is noticed. TABLE 1 shows the total parameter counts of the models with various architectures developed for microstructural categorization within the scope of the study. According to the data shown in Fig. 4, the CNN model with VGG16 architecture, which is the shallowest model with 27 million 825 thousand parameters, has the lowest performance. It was discovered that as the number of parameters rose, so did the success of the models. This performance was seen to decline in models with parameter numbers larger than the parameter number of the top performing DenseNet201 model.

Fig. 5 depicts the confusion matrices derived from the test results, which were applied by picking 100 microstructural images from each class [39]. The vertical axes in the given matrices represent the true label, while the horizontal axes represent the predicted label. When the confusion matrix is examined, four distinct outcomes are expected: true positive (TP), true negative (TN), false positive (FP), and false negative (FN). The number of right predictions given by TP is the number of positive examples given by TP. FP, unlike TP, reports the number of positively predicted but really negative examples. The number of predicted true negatives is given by TN. The number of negative expected but really positive examples is given by FN.

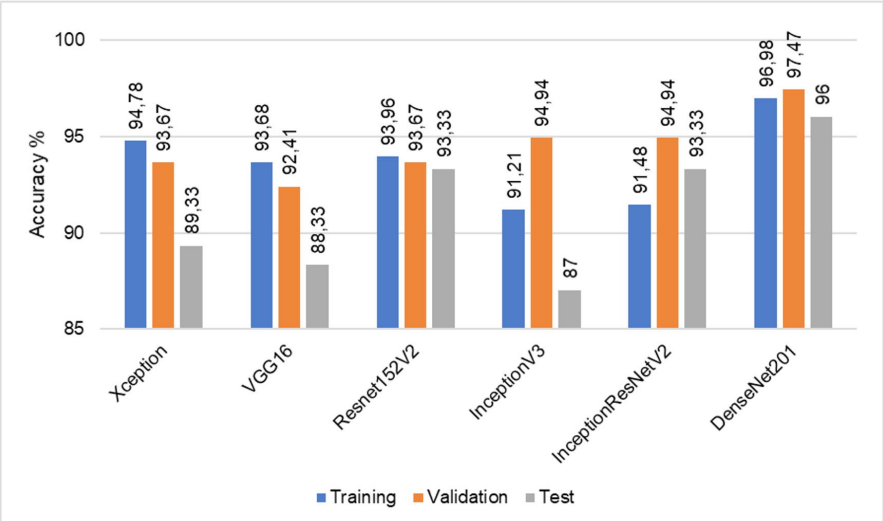

Fig. 4. The model training, validation and test accuracy scores

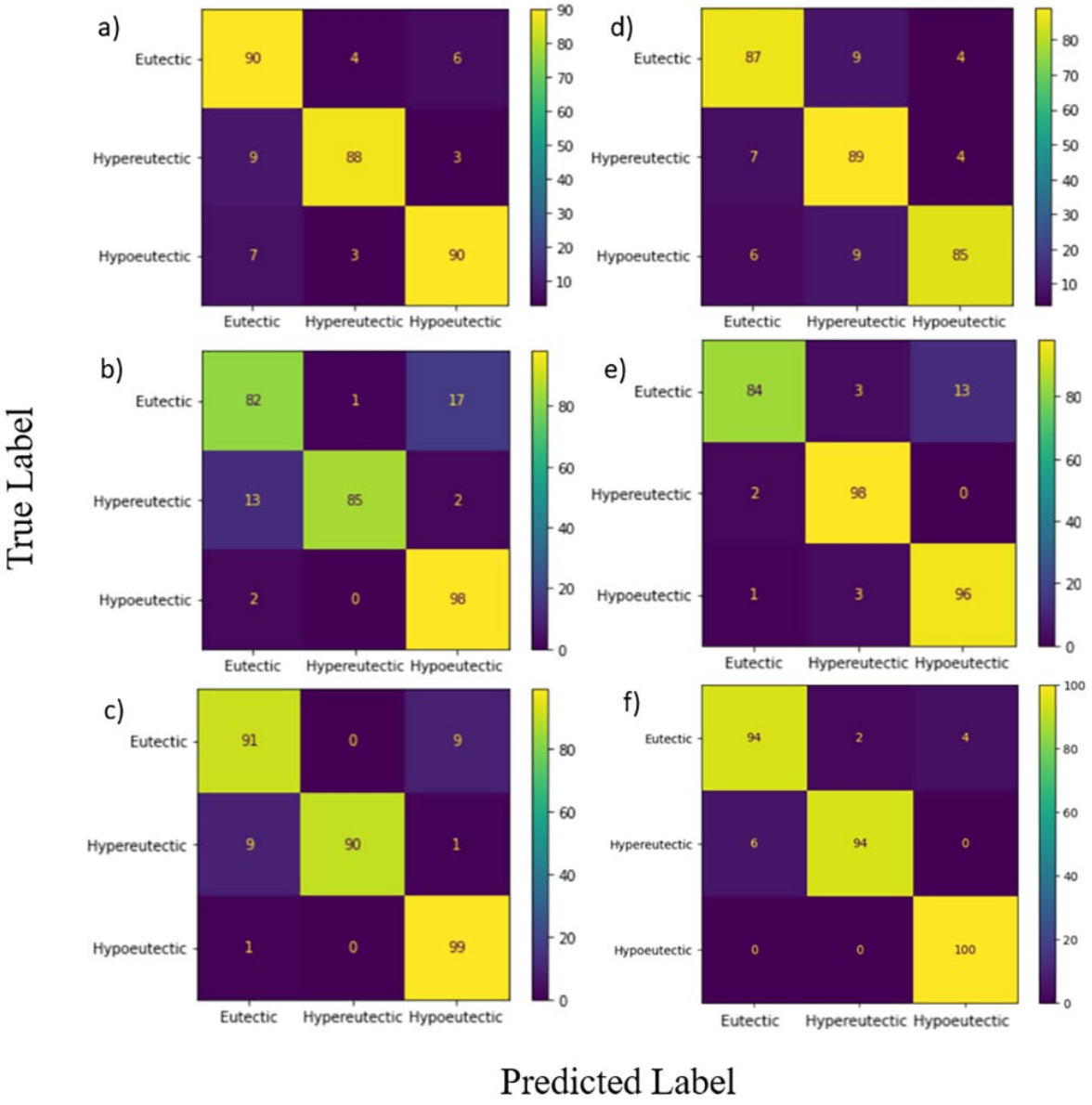

Fig. 5. Confusion Matrix of using a) Xception, b) VGG16, c) Resnet152V2, d) InceptionV3, e) InceptionResNetV2 and f) DenseNet201 architectures

The confusion matrices in Fig. 5 show that all models have a class-based success rate of more than 80%. As the models were tested separately, it was discovered that 17 out of 100 eutectic samples were hypoeutectic, whereas 13 out of 100 hypereutectic samples were eutectic in the model with VGG16 architecture. The false predictions in this model were largely noticed in these two situations, and while it predicted hypoeutectic samples with high accuracy, it was unsuccessful to in the other two groups. It should be highlighted that the same false predictions occur with better outcomes in the ResNet152V2. Similarly, in this model, as in VGG16, the Hypoeutectic class was successful, while the other classes yielded lower outcomes than the Hypoeutectic. Similarly, as like VGG16, the Hypoeutectic class performed well, whereas the other classes performed poorly. While the hypereutectic and hypoeutectic classes appear to be effective in the InceptionResNet152V2 model, the eutectic class was found to be less successful, with erroneous predictions in this class mainly forecasted as hypoeutectic. False predictions were found to be more homogenous but more numerous in the InceptionV3 and Xception models. The DenseNet201 model, on the other hand, had no incorrect predictions in the hypoeutectic class; also, when the eutectic and hypereutectic classes were considered, it was determined that this model made the most consistent predictions.

TABLE 2 is given to show the performance metrics of different machine learning models on a specific task. The metrics were reported as precision, recall, F1-score, and (Area Under The Curve) AUC score. The metrics of precision, recall and F1-score were determined by using confusion matrices of CNN models. Precision is defined as the ratio of estimated TP data to the total of TP and FP data. Precision is particular to the projected outcome from the test data. This metric represents how successfully the model learned positive sample attributes. The higher the precision, the more accurate the forecast of the positive sample looks to be. The recall is calculated as the ratio of the TP number to the total of the TP and FN numbers. The greater the recall rate, the better the prediction of the target sample and the lesser potential

of skipping a poor sample. The F1 score is calculated by averaging the harmonic of precision and recall. In general, accuracy and memory are at odds. As a result, the F1 score balances accuracy and memory effects and gives a composite indicator to evaluate the classifier more correctly [40]. AUC results were obtained using the Scikit-Learn library.

Using the sensitivity, recall, and F1-score criteria, it was discovered that the DenseNet201 model produced the outstanding results, with 0.94. The VGG16 model was determined to be least effective in the proper estimate of positive data, as evidenced in the accuracy results. The value of 0.86 was calculated for the VGG16 model in all three of the precision, recall and F1 scores. The computed precision, recall, and F1-score outcomes of the InceptionResNetV2 and InceptionV3 models were found to be in the same order after the DenseNet201 model as the efficiency performance order. The success order of the models employed in the comparisons based on these three measures is nearly identical to the accuracy findings. According to these data, the only difference detected was that ResNet152V2 produced substantially more sensitive results than the Xception model. This circumstance revealed the opposite based on the accuracy results. In the outcomes of the stated accuracy and other metrics, however, there was no substantial difference in success between these two models. Using the AUC scores, it was established that the findings in this measure, like the results in other metrics, were consistent with the results in other metrics and accuracy.

TABLE 2

The score evaluation with different score values

Model Name	Precision	Recall	F1-Score	AUC
Xception	0.89	0.89	0.88	0.97
VGG16	0.86	0.86	0.86	0.94
Resnet152V2	0.89	0.89	0.89	0.96
InceptionV3	0.92	0.92	0.92	0.98
InceptionResNetV2	0.92	0.91	0.91	0.98
DenseNet201	0.94	0.94	0.94	0.98

4. Conclusion

In this work, a classification method on the microstructure of Al-Si alloys was performed utilizing models created using various CNN architectures. The classification in this study focused on eutectic, hypoeutectic, and hypereutectic Al-Si microstructures, providing valuable insights into the characterization of these samples. The CNN architectures employed were compared based on the classification results. The microstructural images used in this investigation were gathered from a variety of sources. Data augmentation techniques were employed on datasets to provide variations for improving the performance of deep learning classification models. To achieve an appropriate interpretation in the comparison of the architectures, loss curves, accuracy values, precision, recall, F1-Score, and AUC metrics were utilized. The InceptionV3, InceptionResNetV2, and DenseNet201 architectures, in particular, were deemed more successful than other models, with an accuracy of more than 90%. The DenseNet201 architecture was shown to be the most useful classification model after considering all criteria, outperforming the Xception, VGG16, ResNet152V2, InceptionV3, and InceptionResNetV2 designs. Although it has promising findings as the CNN model with DenseNet201 architecture, which has the greatest predictive ability among the models constructed within the scope of the study, the model requires more development in order to better forecast class differences in future investigations.

REFERENCES

[1] M. Yilmaz, H.I. Kurt, N.F. Yilmaz, Manufacturing and Characterization of Al–XMg–XMgO Composites Using Stir Casting Process. Int. J. Met. **17** (3), 2308-2322 (2023). DOI: https://doi.org/10.1007/s40962-022-00946-y

[2] Z. Qiu, K. Sugio, G. Sasaki, Classification of Microstructures of Al–Si Casting Alloy in Different Cooling Rates with Machine Learning Technique. Mater. Trans. **62** (6), 719-725 (2021). DOI: https://doi.org/10.2320/matertrans.MT-MBW2020002

[3] K.J. Kurzydlowski, B. Ralph, The Quantitative Description of the Microstructure of Materials, 1995 CRC Press.

[4] S.P. Mishra, M.R.A. Rahul, Comparative Study and Development of a Novel Deep Learning Architecture for Accelerated Identification of Microstructure in Materials Science. Comput. Mater. Sci. **200**, 110815 (2021)

[5] E.A. Holm, R. Cohn, N. Gao, A.R. Kitahara, T.P. Matson, B. Lei, S.R. Yarasi, Overview: Computer Vision and Machine Learning for Microstructural Characterization and Analysis. Metall. Mater. Trans. A Phys. Metall. Mater. Sci. **51** (12), 5985-5999 (2020). DOI: https://doi.org/10.1007/s11661-020-06008-4

[6] K. Tsutsui, K. Matsumoto, M. Maeda, T. Takatsu, K. Moriguchi, K. Hayashi, S. Morito, H. Terasaki, Mixing Effects of SEM Imaging Conditions on Convolutional Neural Network-Based Low-Carbon Steel Classification. Mater. Today Commun. **32** (July), 104062 (2022). DOI: https://doi.org/10.1016/j.mtcomm.2022.104062

[7] A. Cheloee Darabi, S. Rastgordani, M. Khoshbin, V. Guski, S. Schamuder, Hybrid Data-Driven Deep Learning Framework for Material Mechanical Properties Prediction with the Focus on Dual-Phase Steel Microstructures. Mater. **16** (1), 447 (2023). DOI: https://doi.org/10.3390/MA16010447

[8] Z.L. Wang, Y. Adachi, Property Prediction and Properties-to-Microstructure Inverse Analysis of Steels by a Machine-Learning Approach. Mater. Sci. Eng. A. **744**, 661-670 (2019). DOI: https://doi.org/10.1016/j.msea.2018.12.049

[9] A. Chowdhury, E. Kautz, B. Yener, D. Lewis, Image Driven Machine Learning Methods for Microstructure Recognition. Comput. Mater. Sci. **123**, 176-187 (2016). DOI: https://doi.org/10.1016/j.commatsci.2016.05.034

[10] M. Ji, M. Yang, S. Soghrati, Deep Learning Model to Predict the Failure Response of Steel Pipes under Pitting Corrosion. Comput. Mech. **71** (2), 293-310 (2022). DOI: https://doi.org/10.1007/s00466-022-02238-y

[11] A. Agrawal, Choudhary, Deep Materials Informatics: Applications of Deep Learning in Materials Science. MRS Commun. **9** (3), 779-792 (2019). DOI: https://doi.org/10.1557/mrc.2019.73

[12] V.C Shunmugasamy, E. Khalid, B. Mansoor, Friction Stir Extrusion of Ultra-Thin Wall Biodegradable Magnesium Alloy Tubes – Microstructure and Corrosion Response. Mater. Today Commun. **26**, 102129 (2021).
DO: https://doi.org/10.1016/j.mtcomm.2021.102129

[13] B. Gallagher, M. Rever, D. Loveland, T.N. Mundhenk, B. Beauchamp, E. Robertson, G.G. Jaman, A.M. Hiszpanski, T.Y.J. Han, Predicting Compressive Strength of Consolidated Molecular Solids Using Computer Vision and Deep Learning. Mater. Des. **190**, 108541 (2020). DOI: https://doi.org/10.1016/j.matdes.2020.108541

[14] C. Shen, X. Wei, C. Wang, W. Xu, A Deep Learning Method for Extensible Microstructural Quantification of DP Steel Enhanced by Physical Metallurgy-Guided Data Augmentation. Mater. Charact. **180**, 111392 (2021).
DOI: https://doi.org/10.1016/j.matchar.2021.111392

[15] S. Feng, H. Fu, H. Zhou, Y. Wu, Z. Lu, H.A. Dong, A General and Transferable Deep Learning Framework for Predicting Phase Formation in Materials. npj Comput. Mater. **7** (1), 1-10 (2021). DOI: https://doi.org/10.1038/s41524-020-00488-z

[16] E. Maggiori, Y. Tarabalka, G. Charpiat, P. Alliez, Convolutional Neural Networks for Large-Scale Remote-Sensing Image Classification. IEEE Trans. Geosci. Remote Sens. **55** (2), 645-657 (2017). DOI: https://doi.org/10.1109/TGRS.2016.2612821

[17] F. Chollet, Xception: Deep Learning with Depthwise Separable Convolutions. IEEE Conference on Computer Vision and Pattern Recognition (CVPR). 1800-1807 (2017).
DOI: https://doi.org/10.1109/cvpr.2017.195

[18] M. Shafiq, Z. Gu, Deep Residual Learning for Image Recognition: A Survey. Appl. Sci. **12** (18), 8972 (2022).
DOI: https://doi.org/10.3390/APP12188972

[19] C. Szegedy, S. Ioffe, V. Vanhoucke, A.A. Alemi, Inception-v4, Inception-ResNet and the Impact of Residual Connections on Learning. Proc. AAAI Conf. Artif. Intell. **31** (1), 4278-4284 (2017). DOI: https://doi.org/10.1609/AAAI.V31I1.11231

[20] T. Lu, B. Han, L. Chen, F. Yu, C. Xue, A Generic Intelligent Tomato Classification System for Practical Applications Using DenseNet-201 with Transfer Learning. Sci. Rep. **11** (1), 15824 (2021). DOI: https://doi.org/10.1038/s41598-021-95218-w

[21] H. Barhoumi, S. Souissi, M.B. Amar, F. Elhalouani, Study on the Effect of Pressure and Cooling Rate on the Solidification Characteristics and Mechanical Properties of Al-11% Si Cast Alloy. J. Mater. Env. Sci. **10** (8), 696-705 (2019).

[22] T.H. Ludwig, P.L. Schaffer, L. Arnberg, Influence of Some Trace Elements on Solidification Path and Microstructure of Al-Si Foundry Alloys. Metall. Mater. Trans. A. **44**, 3783-3796 (2013).

[23] K. Wang, P. Tang, Y. Huang, Y. Zhao, W. Li, J. Tian, Characterization of Microstructures and Tensile Properties of Recycled Al-Si-Cu-Fe-Mn Alloys with Individual and Combined Addition of Titanium and Cerium. Scanning. **2018** (2018).

[24] Schmitz Metallographie GmbH Microstructure Database; 2023.

[25] R. Romankiewicz, F. Romankiewicz, Influence of Modification on the Refinement of Primary Silicon Crystals in Hypereutectic Silumin AlSi21CuNi. Prod. Eng. Arch. **19** (19), 30-36 (2018).

[26] Zambon, Phosphorus Modification in Al-Si Hypereutectic Alloys. NTNU 2016.

[27] F. Yu, J. Pei, K. He, D. Zhao, L. Zuo, Solidification Microstructure and Temperature Field during Direct Chill Casting of Al-16Si Alloy. Trans. Indian Inst. Met. **62**, 347-351 (2009).

[28] P. Chokermorh, P. Pandee, C. Limmaneevichitr, Role of Scandium Additions in Primary Silicon Refinement of Hypereutectic Al–20Si Alloys. Int. J. Cast Met. Res. **31** (5), 269-278 (2018).

[29] A. Radjai, K. Miwa, T. Nishio, An Investigation of the Effects Caused by Electromagnetic Vibrations in a Hypereutectic Al-Si Alloy Melt. Metall. Mater. Trans. A. **29**, 1477-1484 (1998).

[30] P. Jiandon, S. Talangkun, Microstructural Modification Hardness and Surface Roughness of Hypereutectic Al-Si Alloys by a Combination of Bismuth and Phosphorus. Crystals. **12** (8), 1026 (2022).

[31] J. Abboud, J. Mazumder, Developing of Nano Sized Fibrous Eutectic Silicon in Hypereutectic Al–Si Alloy by Laser Remelting. Sci. Rep. **10** (1), 1-18 (2020).

[32] R. Pastirčák, J. Ščury, J. Moravec, The Effects of Pressure During the Crystallization on Properties of the AlSi12 Alloy. Arch. Foundry Eng. **17** (3), 103-106 (2017).
DOI: https://doi.org/10.1515/afe-2017-0099

[33] R. Pastirčák, M. Brůna, D. Bolibruchová. The Influence of Different Wall Thicknesses of the Casting in the Direct Squeeze Casting. Arch. Foundry Eng. **19** (1), 19-24 (2019).
DOI: https://doi.org/10.24425/afe.2018.125185

[34] E.M. Elgallad, H.W. Doty, S.A. Alkahtani, F.H. Samuel, Effects of La and Ce Addition on the Modification of Al-Si Based Alloys. Adv. Mater. Sci. Eng. (2016).
DOI: https://doi.org/10.1155/2016/5027243

[35] M.G. Day, A. Hellawell, The Microstructure and Crystallography of Aluminium – Silicon Eutectic Alloys. Proc. R. Soc. London. Ser. A. Math. Phys. Sci. **305** (1483), 473-491 (1968).

[36] J. Lemley, S. Bazrafkan, P. Corcoran, Smart Augmentation Learning an Optimal Data Augmentation Strategy. Ieee Access. **5**, 5858-5869 (2017).
DOI: https://doi.org/10.1109/ACCESS.2017.2696121

[37] E.C. Too, L. Yujian, S. Njuki, L.A. Yingchun, A Comparative Study of Fine-Tuning Deep Learning Models for Plant Disease Identification. Comput. Electron. Agric. **161**, 272-279 (2019).
DOI: https://doi.org/10.1016/j.compag.2018.03.032

[38] F. Chen, J.U. Thou, Assessing the Effects of Convolutional Neural Network Architectural Factors on Model Performance for Remote Sensing Image Classification: An in-Depth Investigation. Int. J. Appl. Earth Obs. Geoinf. **112** ,102865 (2022).
DOI: https://doi.org/10.1016/j.jag.2022.102865

[39] M. Hossin, M.N. Sulaiman, A Review on Evaluation Metrics for Data Classification Evaluations. Int. J. data Min. Knowl. Manag. Process. **5** (2), 1-11 (2015).
DOI: https://doi.org/10.5121/ijdkp.2015.5201

[40] D. Krstinić, M. Braović, L. Šerić, D. Božić-Štulić, Multi-Label Classifier Performance Evaluation with Confusion Matrix. Comput. Sci. Inf. Technol. **2020**, 1-14 (2020).
DOI: https://doi.org/10.5121/csit.2020.100801